FIELD TESTING OF AGUASABON RIVER BRIDGE IN ONTARIO

J. Peter C. King and Paul F. Csagoly,
Ontario Ministry of Transportation and Communications; and
John W. Fisher, Lehigh University

This paper describes the field testing of the Aguasabon River bridge in Ontario, a three-span, continuous, steel girder bridge with parabolic haunches of composite concrete slab construction. As part of the 1973 bridge testing program, the structure was tested both statically and dynamically with two load-testing vehicles. Because this structure had a history of failures of the haunch weld detail and because it was one of several similarly designed structures, it was decided to determine the actual bridge behavior under load as well as its structural adequacy. Outlined are the grid type and other analytical procedures followed to predict stresses and deflections, which are then compared with those values recorded during the static loading. An estimate of the fatigue life of the weld details is made by using the dynamic strain data obtained. General aspects of the behavior of the structure are discussed, and conclusions are drawn on the structural adequacy of the test bridge and the methods used in the analysis and testing.

•THE Ministry of Transportation and Communications, Ontario, has a continuing load-testing program in which about 10 structures are analyzed and load tested each year. This program is designed primarily to determine safe load-carrying capacity of some of the suspect structures of the more than 13,000 highway bridges in the province. To expand the knowledge on the behavior of highway structures under load, these bridges are subjected to rigorous testing. Extensive instrumentation is used and suitable test conditions are provided so that comparison can be made between current design-analytical techniques and actual field results.

The Aguasabon River bridge in northern Ontario was in the 1973 bridge testing program primarily because it had severe weld cracks at three locations on one girder. Because it is one of several similarly designed bridges, it was felt extensive testing of it would give a better understanding of the structural behavior of all these bridges.

STRUCTURAL DESCRIPTION

The Aguasabon River bridge is located on the north shore of Lake Superior on Highway 17 (Trans-Canada Highway), 130 miles (210 km) east of Thunder Bay, Ontario. The three-span, continuous structure, built in 1948, is of composite beam-slab construction designed by the Ontario Department of Highways for an H20 truck load.

The 200-ft (61-m) structure (Figure 1) consists of four 33-in. (84-cm) WF girders, haunched at both piers and abutments. These haunches were fabricated by cutting the bottom flange at the web fillet and welding a parabolic insert, which resulted in a 51.25-in. (1.30-m) section at the piers and abutments (Figure 2).

In 1963, severe cracks, one of them extending 44 in. (1.12 m) into the web along a diagonal line, were found at the vertical weld detail in three of the six haunch inserts of the north interior girder. These cracks were repaired by welding cover plates or insert plates in a fashion similar to that shown in Figure 3. Prior to the 1973 tests, dye-penetrant and magnetic-particle weld inspection techniques were used on the repairs and the 21 remaining vertical welds, with the result that four other weld cracks were discovered. Figures 4, 5, and 6 show two of these weld cracks. The cracked vertical

Figure 1. Aguasabon River bridge.

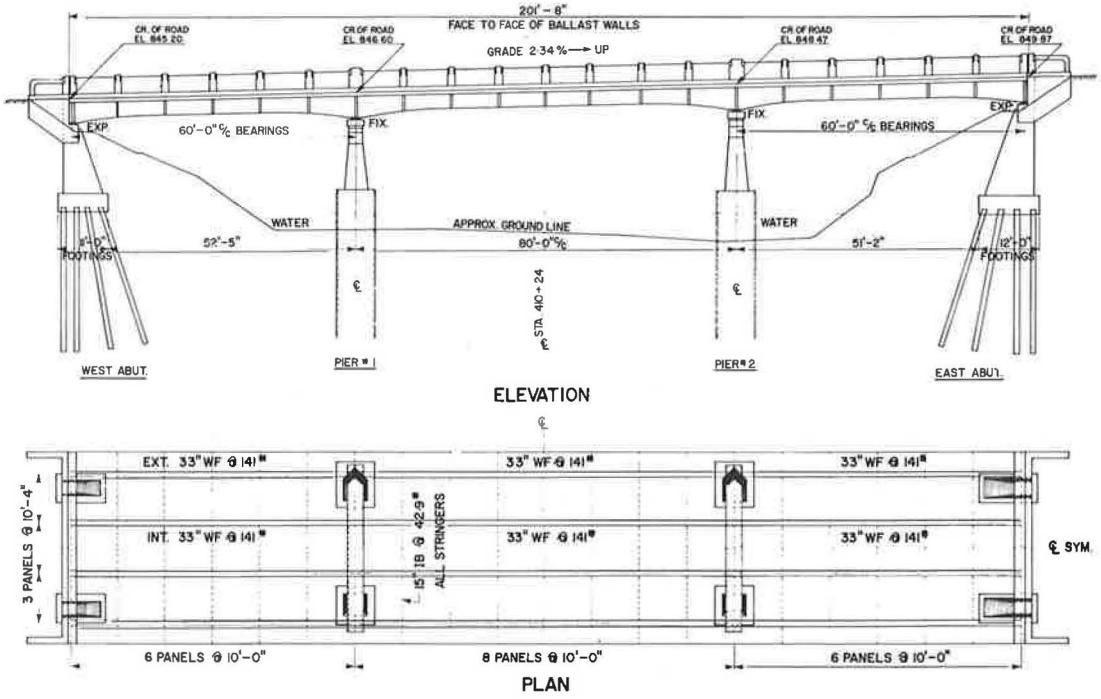

Figure 2. Shear connector and haunch details.

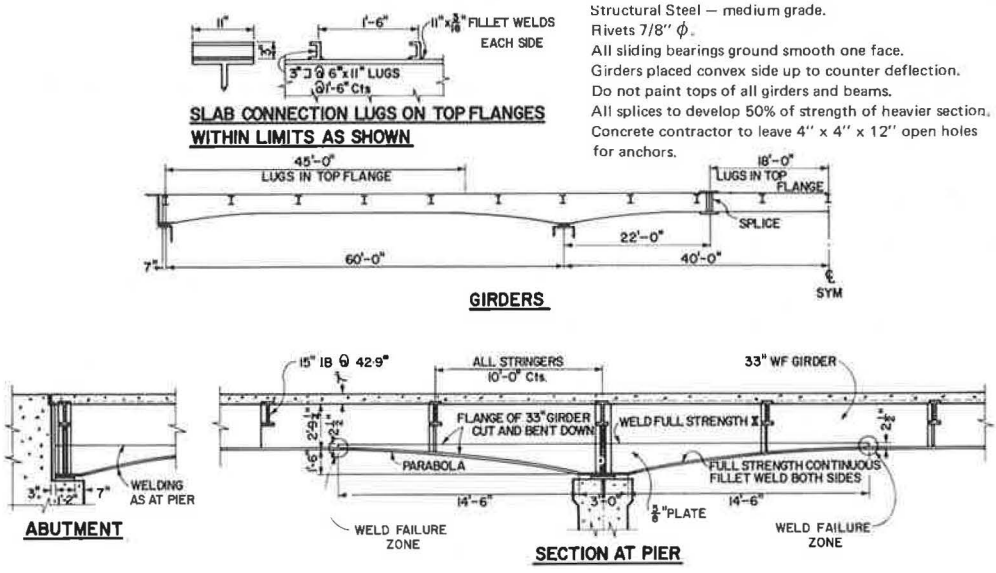

Structural Steel — medium grade.
Rivets 7/8" ϕ.
All sliding bearings ground smooth one face.
Girders placed convex side up to counter deflection.
Do not paint tops of all girders and beams.
All splices to develop 50% of strength of heavier section.
Concrete contractor to leave 4" x 4" x 12" open holes for anchors.

weld area was cut out in a circular shape, and an insert was welded in its place. Where the crack had penetrated the bottom flange, it was gouged out and filled with weld material, at a slow rate of deposit, by using low-hydrogen-coated electrodes. All repaired surfaces were subsequently ground flush to eliminate any stress risers.

The girders are field spliced at two points in the interior span 22 ft (6.7 m) from each pier, theoretically at the points of dead load contraflexure. Field personnel noted that the riveted splice consisted of $\frac{5}{8}$-in. (16-mm) flange plates on the interior and $\frac{1}{2}$-in. (12.7-mm) plates on the exterior girders. All had two $\frac{3}{8}$-in. (10-mm) web plates for the shear splice. Details of the field connection are shown in Figure 3.

The deck system consists of nominal 7-in.-thick (178-mm) two-way reinforced slab panels, continuous over adjacent girders, and 15-in. (381-mm) I-shape floor beams. The floor beam-to-girder connection serves as a vertical stiffener in addition to a shear transfer from floor beam to girder. Channel types of shear connectors were used in the regions of positive dead load moment to ensure composite action.

The piers are of the two-column bent type with concrete-filled sheet pile caissons. The abutments are similar in design but are supported by timber piles. There are no abutment walls, and consequently the fill behind the east abutment has slipped and has undermined the support beam and created a rough approach to the structure. The substructure is generally in good condition except that on the east abutment some of the reinforcing steel is exposed because of excessive spalling of the concrete.

A network of scaffolding was erected beneath the structure to enable free access to all weld and splice areas and to provide a working platform for inspection and instrumentation.

ANALYTICAL TECHNIQUES

The Ministry's Structural Research Section has at its disposal two load-testing vehicles, each capable of carrying a maximum payload of 153,000 lb (69 400 kg) with a gross vehicle weight (GVW) of 197,000 lb (89 350 kg) on five axles. This payload in turn can be placed on the semitrailer in such a manner as to produce any desired tandem axle weight of up to 110,000 lb (49 900 kg). The base length is 52 in. (1.32 m).

The analytical tools outlined above were used to determine the maximum test loads and critical vehicle positions based on a permissible maximum bending stress in the structural steel of 30 ksi (207 MPa).

Superstructure

A multiple-girder grid analysis computer program was developed by the Structural Research Section to determine bending moment, shear, reaction, or displacement of a multigirder bridge under a series of moving or static loads. The use of both transverse and longitudinal strips instead of finite elements as in other more general computer programs reduces the number of unknowns at each node to one, vertical displacement (1). This drastically reduces the amount of computation necessary to obtain the parameters mentioned above. The live load stresses resulting from the application of this program were combined with the computed dead load stresses to arrive at several load positions for maximum stresses at midspan, at the eastern pier, and at the end span for each of the four girders.

Web cutouts, taken from the weld failure zones (Figure 2), were analyzed to determine their chemical composition. Moreover, an examination of the fracture surfaces revealed that they were indeed fatigue cracks originating at extremely large initial weld imperfections and inclusions. Results of the chemical analysis of the base material (A7 steel) were as follows:

Chemical	Percent	Chemical	Percent
Carbon	0.24	Phosphorous	0.01
Manganese	0.74	Sulfur	0.03
Silicon	0.09		

Substructure

A working stress analysis was performed on both piers and abutments by using the vehicle configurations described above. Abutment stresses were within acceptable limits, but the stress in the pier tension reinforcement was extremely high when two fully loaded vehicles were located directly over the pier.

Proposed Test Loads and Test Procedure

As in all forms of structural analysis, many assumptions must be made to establish the load-carrying capacity of a bridge without expending an undue amount of time and effort. Thus this analysis should be supplemented by a careful testing procedure to prevent a catastrophic failure. Two fully loaded vehicles each with a GVW of 197,000 lb (89 360 kg) were approved through the Ministry's standard evaluation procedures as the maximum test loads. These loads were to be applied in four increments while stresses were monitored at the critical areas. The pretest analysis of the structure was used to determine both the maximum test loads and those areas in which stresses may be critical during testing.

Later in this paper, comparisons are made between the test results and the predicted stresses and moments (Table 1). The test load positions for the desired load increments are given in Table 2. These positions are shown in Figure 7.

INSTRUMENTATION

Figure 8 shows the location of the instrumentation used to measure all strains and deflections.

Deflection Measurement

Two theodolites of 1-sec resolution were used to determine deflection by triangulation. In the 50 to 100-ft (15 to 30-m) range in which they were used, an accuracy of ±0.006 in. (±0.15 mm) could be obtained. Because the structure is continuous over the piers and the pier reinforcement was expected to be highly stressed, pier settlement or deflection was also monitored. Without this information, the test results could never be correlated with analytical strains because of the severe effect any movement would have on the distribution of moments. Deflection targets were mounted on the east pier and abutment, at midspan, and at six locations in the end span on all four girders.

Strain Measurement

Thirty-four SR-4 electrical resistance strain gauges were mounted in pairs on the steel girders so that sectional bending moment values could be obtained. One gauge was mounted on the top of the bottom flange and the other on the bottom of the top flange. These were wired in a half active Wheatstone bridge configuration, with bridge completion in the instrumentation van. All but three were used to measure static strain.

These three, as well as an additional three gauges, were monitored through a set of dc high-gain operational amplifiers driving a multichannel light-beam oscillograph.

Figure 3. First north interior field splice and repair to weld failure (1963).

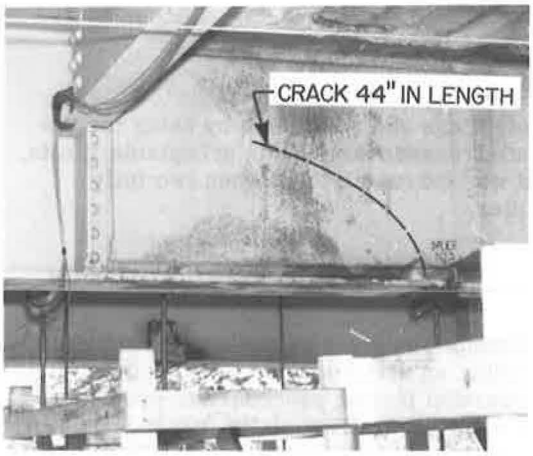

Figure 4. Dye-penetrant crack detection in fourth north exterior weld detail.

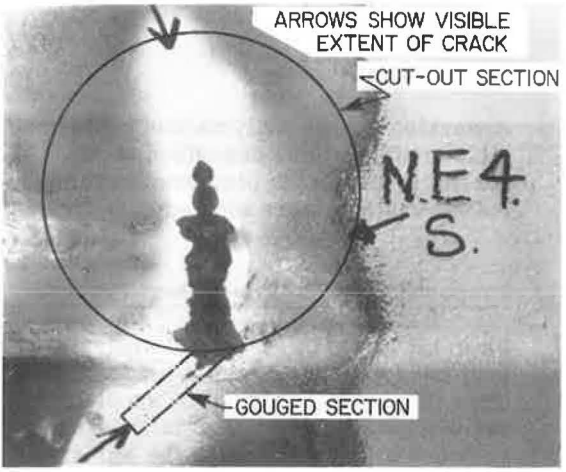

Figure 5. Cutout section of fourth north exterior weld detail.

Figure 6. Cutout section of second north exterior weld detail.

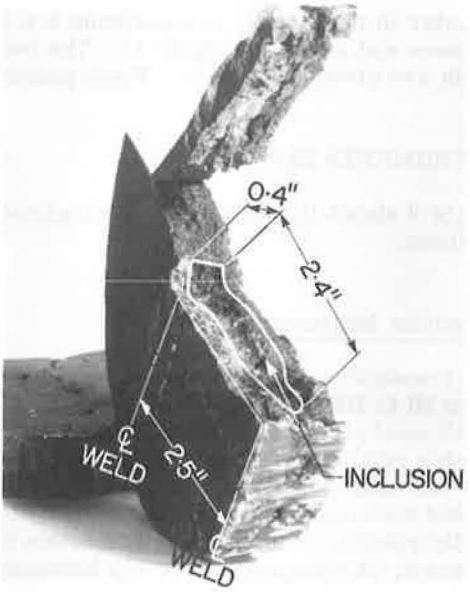

Table 1. Expected maximum live load stresses.

Location	Expected Stresses (ksi)		
	Live	Dead	Total
24-ft maximum end span	-20.1	-9.0	-29.1
44-ft second haunch weld detail	-15.8	+2.5	-13.3
60-ft east pier	+17.4	+14.1	+31.5
80-ft splice zone	-13.9	-2.0	-15.9
100-ft center span	-20.6	-10.5	-31.1

Note: 1 ft = 0.3 m; 1 ksi = 6.9 MPa.
"- = tensile stress; + = compressive stress.

Figure 7. Test positions identified in Table 2.

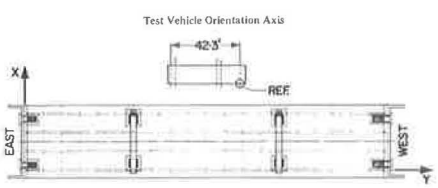

Several hours of continuous dynamic strain data were recorded by means of an FM tape recorder paralleling the light-beam oscillograph. The dynamic gauges were used in the static as well as in the dynamic tests so as not to lose any bending test data. An additional 12 gauges were used to monitor stress at several critical locations (Figure 8). Another strain gauge was mounted on a small block of steel, placed beneath the structure, to serve as an indication of instrument or temperature-induced drift.

TEST PROCEDURE

Dynamic Tests

To determine the fatigue life of the structure requires that its response to a typical heavy vehicle and the statistical distribution of the vehicle population be known. Recordings were made of dynamic strains as the test vehicle, loaded to a gross weight of 91,000 lb (41 280 kg), crossed the bridge at speeds varying from 30 to 50 mph (48 to 80 km/h). This information was used to select the most active gauges for the purpose of recording as well as an actual calibration of the dynamic strain system. Test data were recorded for $32\frac{1}{2}$ hours throughout the testing period.

Static Tests

The first series of tests was carried out with 36 load blocks (2,125 lb or 964 kg per block) on board each test vehicle or a GVW of 122,000 lb (55 340 kg). The strains recorded were generally well below those anticipated. The maximum was 341 μin./in. or 10.3 ksi (71.0 MPa). Because a number of vehicle positions were similar for different tests, several were combined into a single test and others were omitted, mainly because of a lack of time.

Strains measured in the first north interior (NI1) splice plate up until test 5B were roughly twice those found in the corresponding plate on the north exterior (NE) girder [maximum tensile and compressive strain ±77 μin./in. or ±2.7 ksi (18.62 MPa)]. It was observed during the positioning of the secondary vehicle (i.e., test 5B) that the strain gauge affixed to the NI1 splice plate indicated strains of 752 μin./in. or 26 ksi (179.3 MPa). Also, a loud, explosion-like sound was heard by those beneath the structure, and it was assumed to have come from the region of the central span. When the load was removed, a permanent set of 634 μin./in. or 22 ksi (151.7 MPa) was indicated by the strain-measuring instruments if the elastic modulus applied. The remaining gauges indicated that elastic strains existed in the rest of the structure.

To clarify the questionable results from this splice plate, an additional strain gauge was attached near the first and was monitored throughout the second day of testing. When the load was increased to 147,000 lb (66 680 kg) on each vehicle (48 test series) a similar situation was encountered. The explosive sound was heard, louder than before, and plate stresses this time reached 38 ksi (262.0 MPa) or 1,095 μin./in. with a permanent offset of 940 μin./in. The second strain gauge confirmed the readings obtained from the original one. A number of repeated loadings were made with plate movements measured by precision dial gauges, and a similar elastic strain was recorded with increasing permanent set each time. This confirmed suspicions that the splice plate had undergone considerable yielding. The remainder of the tests were completed at this load value, but test series 60 and 72 were abandoned because there was fear that serious structural damage would result. Figure 9 shows a typical loading condition of test series 48.

Table 2. Test vehicle positions.

Maximum Moment		Test	Vehicle Location					
			Primary A			Secondary B		
Location	Sign	Number	X	Y	Direction	X	Y	Direction
End span, 24 ft								
Exterior	+	1	0.67	58.33	West	15.67	58.33	West
Interior	+	2	5.67	56.33	West	15.67	58.33	West
Pier, 60 ft								
Exterior	+	3	0.67	118.33	West	0.67	64.33	West
Interior	+	4	6.67	31.67	East	4.67	75.67	East
Center span, 78 ft								
Exterior	+	5	0.67	61.67	East	15.67	71.67	East
Interior	+	6	4.67	61.67	East	15.67	61.67	East
Exterior	-	7	0.67	5.67	East	15.67	3.67	East
Interior	-	8	0.67	5.67	East	15.67	5.67	East
Center span, 100 ft								
Exterior	+	9	0.67	136.33	West	15.67	128.33	West
Interior	+	10	4.67	138.33	West	15.67	136.33	West
First interior floor beam	+	11	4.67	50.00	West	15.67	50.00	West

Note: 1 ft = 0.3 m.

Figure 8. Instrumentation.

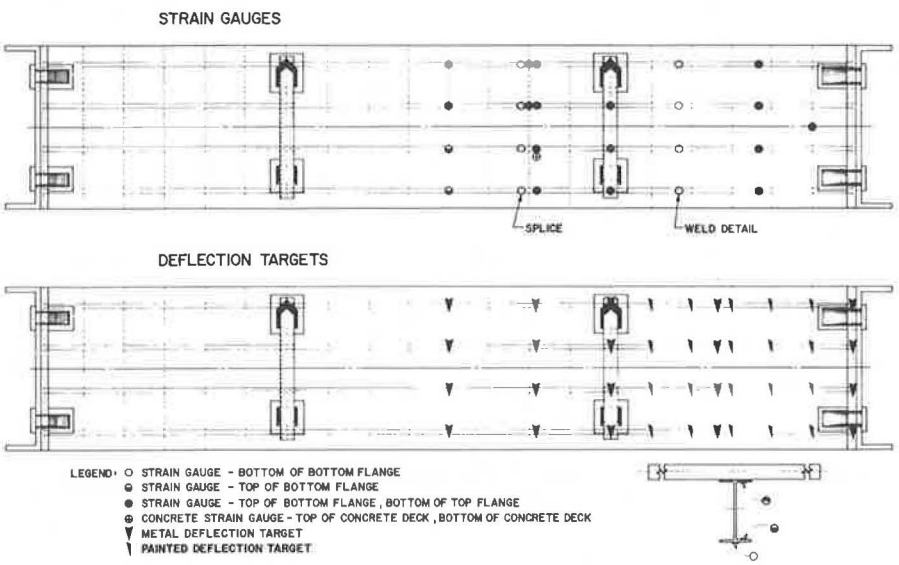

Figure 9. Test 1B-48 maximum moment at east end span.

DATA ANALYSIS

Deflections

The use of triangulation techniques to reduce all deflection data resulted in the deflected shape of the structure under load. Measured deflections were compared to revised deflection results from the multigirder computer program by using loading conditions identical to those used in the field. The maximum recorded deflection was 0.756 in. (19.2 mm) at the center span with a 244,000-lb (110 680-kg) live load on the structure in comparison with the revised calculated deflection of 0.732 in. (18.6 mm). Pier and abutment displacements were negligible. Deflection distribution factors similar to the AASHTO load distribution factors, in terms of girder spacing (2), are given in Table 3.

Static Strains

Sectional values of bending moment were obtained from strain data recorded at two locations (A and B in Figure 10a) for each pair of strain gauges. Two major assumptions were made in this analysis:

1. The distribution of strains throughout the slab and the steel girder is linear, and
2. The steel girder and the slab deflect equal amounts at all test points (i.e., equal curvatures, thus parallel strain distributions in the slab and beam).

Expressions can be derived as outlined in the appendix[1] relating measured strains and the internal forces acting within the partially composite section (3), and sectional bending moments were easily calculated. These in turn were compared with revised multigirder program runs with the actual loading conditions. Distribution factors were derived in a manner similar to that used for deflection. The effect of slip between the girder and slab on the distribution of strain throughout the composite section is currently under investigation by the Structural Research Section. This study may aid in clarifying the behavior of composite structures such as the Aguasabon River bridge.

Dynamic Strains

Figure 11 shows three typical strain records made when the test vehicle was traveling at 45 mph (72 km/h) in the eastbound lane. These and other traces were examined, and a representative histogram of stress range (S_r) was determined (Figure 12). The service life of the welded details of the Aguasabon River bridge was estimated from the measured stress range histogram and the estimated fabricated flaw conditions that existed in the structure.

The stress range histogram was used to estimate the root mean square stress range S_{rRMS} for various minimum stress range conditions. When all stress range levels greater than 0.85 ksi (5.9 MPa) were considered, this resulted in S_{rRMS} = 1.92 ksi (13.2 MPa) at an annual rate of 1,340,000 cycles. This also provided a lower life estimate than when smaller stress range levels were considered.

Service life was estimated from the crack growth relationship developed for welded steel details (8, 9). The semiempirical differential equation of crack growth was taken as

[1] The original manuscript included an appendix on determining strain relationships. That appendix is available in Xerox form at cost of reproduction and handling from the Transportation Research Board. When ordering, refer to XS-66, Transportation Research Record 579.

Table 3. Deflection distribution factors.

Test	24 Ft		78 Ft		100 Ft	
	Deflection Distributor Factor[a]	Deflection[b]	Deflection Distributor Factor	Deflection	Deflection Distributor Factor	Deflection
1A-36	0.491	0.055				
1A-48	0.846	0.026				
1B-48	0.339	0.124				
2A-36	0.331	0.046				
5A-36			0.412	0.085	0.407	0.118
5B-36			0.333	0.129	0.317	0.199
5A-48			0.365	0.074	0.404	0.109
6A-48			0.417	0.084	0.373	0.118
6B-48			0.366	0.172	0.341	0.226
7A-48			NA	NA	0.379	0.029
9A-36			0.367	0.060	0.400	0.095
9B-36			0.336	0.125	0.335	0.194

Note: 1 ft = 0.3 m.

[a]Percentage girder with greatest deflection is of sum of all four deflections.
[b]Sum of all four deflections at a single cross section.

Figure 10. Composite T-beam with incomplete interaction (slip): (a) cross section, (b) forces, and (c) strain distribution.

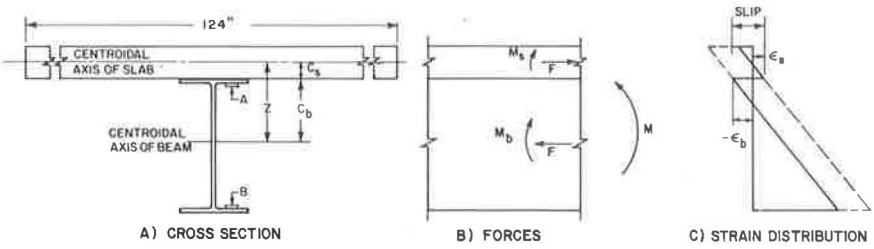

Figure 11. Typical dynamic response.

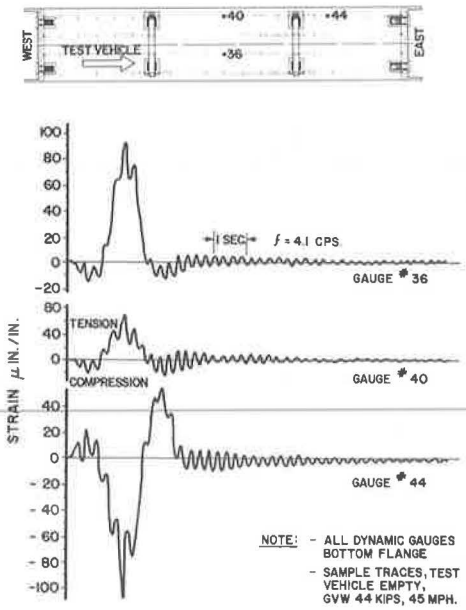

$$da/dN = 2 \times 10^{-10} \Delta K^3 \quad (1)$$

The stress intensity factor was estimated for two stages of crack growth. The first corresponded to the internal weld discontinuity (inclusion) that was fabricated into the vertical groove welds. The fabricated discontinuity was assumed to provide an initial crack condition. The embedded discontinuity was assumed to act as an embedded elliptical crack perpendicular to the bending stress field. For this stage of crack growth, K was estimated as

$$K = \frac{\sigma}{\phi_o} \sqrt{\pi a} \sqrt{\text{Sec} \frac{\pi a}{t}} \quad (2)$$

where

σ = bending stress,
a = half the minor diameter of the elliptical crack,
t = thickness of the weld (0.8 in. or 20 mm), and
ϕ_o = elliptical integral that depends on the minor-to-major axis ratio of the crack.

After the fatigue crack had penetrated the web weld thickness, the remaining life was estimated by assuming that the web crack propagated through the flange as a penny-shaped crack. This model has been demonstrated to be applicable to crack growth in welded beams that experience crack growth from internal flaws in the web-flange welded connection (8). It has also been used to estimate the interval of life for stiffeners welded to the web alone after the fatigue crack had penetrated the web thickness (9). The K-value was taken as

$$K = \frac{2}{\pi} \sigma \sqrt{\pi a} \sqrt{\text{Sec} \frac{\pi a}{2r}} \quad (3)$$

for this stage of growth, where r is the distance from the origin to the bottom of the flange surface.

The life intervals for the two stages of growth were estimated from equations 1, 2, and 3, which resulted in

$$N = \frac{10^{10}}{2} \int_{a_i}^{a_f} \frac{da}{\Delta K^3} \quad (4)$$

During the first stage of growth, the life interval N_1 was estimated by assuming that growth occurred in the direction of the minor axis 2a with a relatively constant major axis 2b, until the weld surface was penetrated (Figure 13). The second stage of growth, in which a penny-shaped crack was assumed, was used until the crack had penetrated the bottom flange thickness.

S_{rRMS} was used to describe the random variable stress field inasmuch as recent studies have shown that it is a satisfactory method for relating constant and variable cycle loading (10, 11). Hence, when ΔK was defined in terms of equations 2 or 3, S_{rRMS} was used for σ.

The results of the analysis (Table 4) revealed that S_{rRMS} = 1.92 ksi (13.2 MPa), and an annual rate of 1,340,000 stress cycles provided the least life prediction. For the inclusion shown in Figure 4, it was estimated that approximately 3½ years would be required before the crack penetrated the bottom flange surface during the first stage of

crack growth. An additional 20 years would be required before the crack penetrated the bottom flange surface during the second stage of crack growth.

The same inclusion was also examined for other locations in the web weld. If the inclusion were centered in the web, as many as 20 years could be required to penetrate the web surface. Smaller inclusions would obviously require a greater time interval (Table 4).

The results of the analysis are in good agreement with field experience with these welded details. The first cracked details were detected in 1963 after about 15 years of service and in all probability had a more severe initial discontinuity than the detail analyzed. An increase in the discontinuity size would decrease the life expectancy. Of the four cracks detected in 1973 after 25 years of service, only one had completely penetrated the bottom flange surface. Given an estimated life expectancy of between 23 and 40 years, these various stages of crack growth are comparable. Details that have no visible damage may have internal cracks that have not yet penetrated the web surface.

Because the weld inclusions far exceeded the level of internal discontinuities that are permitted at groove weld transverse to the bending stress field, the allowable design stress range is not applicable to these details. The design value is based on and assumes normal fabrication conditions, which were not present (4). Hence, comparisons with past or present design conditions provide no insight into the performance of these joints.

DISCUSSION OF TEST RESULTS

Discussions of continuous steel girder bridges have been written by the designer of the Aguasabon River bridge (6, 7). He states that the splice plates are designed for 50 percent of the capacity of the steel girder (WF section). By current specifications, this value appears to be very low; a minimum of 75 percent is now required (2).

Because in test 5B-48 the recorded stress was in excess of that required for yield, it is safe to assume that at least some of the residual strain recorded was due to plastic deformation in the splice material. This theory is further confirmed by tests made with precision dial gauges, which showed that the splice plates slide to a varying extent under a moving load and then hang up on rivets. It was when this movement was prevented that the high stresses were recorded in the splice plate.

The multigirder program requires inertia, torsional stiffness of the exterior girders, and diaphragm stiffness values as input to mathematically describe the structure. As might be expected, any variation in these parameters makes a significant change in computed deflections and moments. The first trial using inertias suggested by AASHTO provided poor agreement with the experimental deflected shape. However, by increasing the inertias in the negative dead load bending moment region, the computed deflections approached the experimental cross-sectional average. The final inertias used corresponded to a fully composite deck throughout the length of the bridge, with 80 percent of the slab width effective. Further variation of the floor beam stiffnesses and the torsional stiffness of the exterior girder would provide better transverse agreement. Correlation between experimental and theoretical moments was not consistent. Good agreement was obtained at midspan, and poor to fair agreement was obtained elsewhere. Figures 14 and 15 show the agreement obtained for test 5A-36 for both deflection and moment respectively.

As many as 20 bridges in the province of Ontario were constructed in the late 1940s by using a design similar to that of the Aguasabon River bridge. Based on the tests, a thorough inspection and analysis of each structure were undertaken. Of these structures, seven were found to have substandard splices and nine were found to have weld details that were prone to fatigue cracking. Subsequently, all of the splices were structurally reinforced and all of the suspect weld zones were repaired.

Figure 12. Stress range histogram (smoothed).

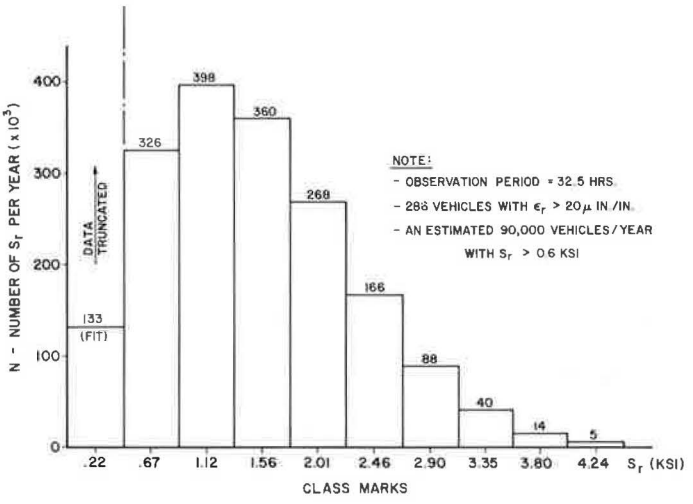

Figure 13. Assumed stages of crack growth.

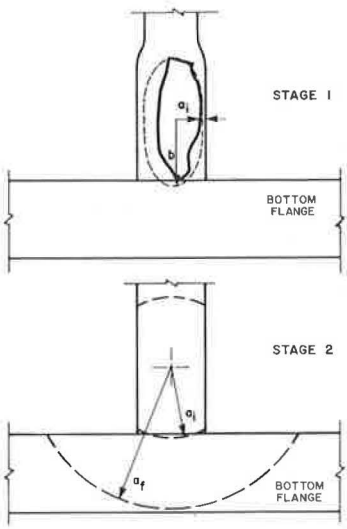

Table 4. Summary of estimated life.

Cracking Stage	Initial Crack Size (in.)	Initial Crack Radius (in.)	Stress Cycles (S_{rRMS} = 1.92 ksi)	Years to Achieve
Crack growth through web	0.25		25,360,000	18.9
	0.30		8,175,000	6.1
	0.32		4,500,000	3.4
Crack growth through flange		1.40	31,700,000	23.6
		1.45	26,200,000	19.6
		1.50	21,400,000	16.0

Note: 1 in. = 2.5 cm; 1 ksi = 6.9 MPa.

Figure 14. Deflected shape.

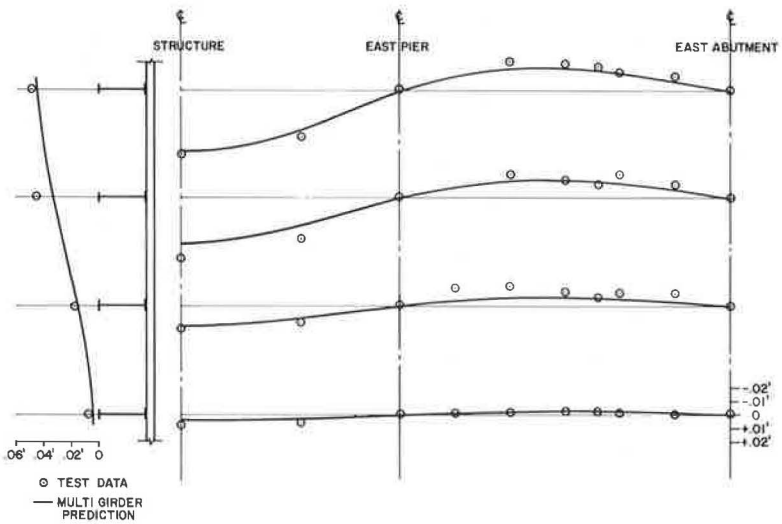

Figure 15. Cross-sectional moment distribution.

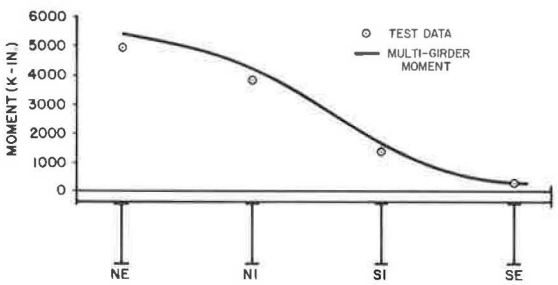

CONCLUSIONS

1. Throughout testing, commercial traffic using the structure consisted of a consisted of a considerable number of six-axle vehicles with an estimated gross weight of 112,000 lb (50 900 kg). With a 35 percent impact factor, these vehicles are imposing high cyclic stresses equal to or in excess of those in series 48 tests. Thus, the splice plates are damaged continually, which promotes crack growth and eventual failure.
2. From the evaluation of the experimental data, fatigue failures at the vertical groove welds in the beam web were inevitable with the large weld inclusions fabricated into the structure. With proper welding techniques the fatigue strength of the structure would be more than adequate.
3. A more detailed study of slab stresses could be carried out to better arrive at values of composite inertia. Slip between the steel and concrete could also be measured to provide a further check on the assumption of linear strain throughout the semicomposite section.
4. To satisfactorily model the structural behavior under load required that a value of 80 percent effective width of the deck slab be assumed. This value was used throughout the full length of the structure, even in the regions designed as noncomposite. This assumption could be substantiated by further tests of continuous structures with particular attention paid to slab and reinforcing steel stresses in the negative moment regions.

REFERENCES

1. P. F. Csagoly, C. Y. Chung, and B. Bakht. Computer Program for the Analysis of Multi-Girder Bridges. Ministry of Transportation and Communications, Downsview, Ontario.
2. Standard Specifications for Highway Bridges. American Association of State Highway Officials, 1973.
3. C. P. Siess, I. M. Viest, and N. M. Newmark. Studies of Slab and Beam Highway Bridges: Part III. Engineering Experiment Station, Univ. of Illinois, Bulletin Series 396, Vol. 49, No. 45, Feb. 1952, pp. 115-133.
4. J. W. Fisher, K. H. Frank, H. A. Hirt, and B. M. McNamee. Effect of Weldments on the Fatigue Strength of Steel Beams. NCHRP Rept. 102, 1970.
5. M. A. Miner. Cumulative Damage in Fatigue. Journal of Applied Mechanics, Vol. 12, No. 1, Sept. 1945.
6. L. Loch. Bridges Over Railways. Roads and Bridges, Nov. 1947.
7. L. Loch. Continuous Steel Girder Bridges. Roads and Bridges, Feb. 1947.
8. M. A. Hirt and J. W. Fisher. Fatigue Crack Growth in Welded Beams. Engineering Fracture Mechanics, Vol. 5, 1973, pp. 415-429.
9. J. W. Fisher, P. A. Albrecht, B. T. Yen, D. J. Klingerman, and B. M. McNamee. Fatigue Strength of Steel Beams With Welded Stiffeners and Attachments. NCHRP Rept. 147, 1974.
10. J. M. Barsom. Fatigue-Crack Growth Under Variable Amplitude Loading in ASTM A514 Grade B Steel. ASTM, STP 536, 1973.
11. C. G. Schilling, K. H. Klippstein, J. M. Barsom, and G. T. Blake. Fatigue of Welded Steel Bridge Members Under Variable-Amplitude Loadings. NCHRP, Research Results Digest 60, April 1974.